Solution Structure of a Wedge-Shaped Synthetic Molecule at a Two-Base Bulge Site in DNA†

Geum-Sook Hwang,‡ Graham B. Jones,§ and Irving H. Goldberg*,‡

Department of Biological Chemistry and Molecular Pharmacology, Harvard Medical School, Boston, Massachusetts 02115, and Bioorganic and Medicinal Chemistry Laboratories, Department of Chemistry, Northeastern University, Boston, Massachusetts 02115

Received March 21, 2003

ABSTRACT: The solution structure of the complex formed between an oligonucleotide containing a two-base bulge (5′-CACGCAGTTCGGAC•5′-GTCCGATGCGTG) and DDI, a designed synthetic agent, has been elucidated using high-resolution NMR spectroscopy and restrained molecular dynamic simulation. DDI, which has been found to modulate DNA strand slippage synthesis by DNA polymerase I [Kappen, L. S., Xi, Z., Jones, G. B., and Goldberg, I. H. (2003) *Biochemistry 42*, 2166−2173], is a wedge-shaped spirocyclic molecule whose aglycone structure closely resembles that of the natural product, NCSi-gb, which strongly binds to an oligonucleotide containing a two-base bulge. Changes in chemical shifts of the DNA upon complex formation and intermolecular NOEs between DDI and the bulged DNA duplex indicate that agent specifically binds to the bulge site of DNA. The benzindanone moiety of DDI intercalates via the minor groove into the G7-T8-T9•A20 pocket, which consists of a helical base pair and two unpaired bulge bases, stacking with the G7 and A20 bases. On the other hand, the dihydronaphthalenone and aminoglycoside moieties are positioned in the minor groove. The aminoglycoside, which is attached to spirocyclic ring, aligns along the A20T21G22 sequence of the nonbulged strand, while the dihydronaphthalenone, which is restrained by the spirocyclic structure, is positioned near the G7-T8-T9 bulge site. The aminoglycoside is closely aligned with the dihydronaphthalenone, preventing its intercalation into the bulge site. In the complex, the unpaired purine (G7) is intrahelical and stacks with the intercalating moiety of DDI, whereas the unpaired pyrimidine (T8) is extrahelical. The structure of the complex formed by binding of the synthetic agent to the two-base bulged DNA reveals a binding mode that differs in important details from that of the natural product, explaining the different binding specificity for the bulge sites of DNA. The structure of the DDI-bulged DNA complex provides insight into the structure−binding affinity relationship, providing a rational basis for the design of specific, high-affinity probes of the role of bulged nucleic acid structures in various biological processes.

Bulge structures in nucleic acids, involving one or more unpaired bases, are of general biological significance and are potential targets for therapeutic drugs (*1*−*4*). They may arise as a consequence of recombination between chromosomal segments that are imperfectly homologous, or of slipped mispairing during the replication of DNA, and may be involved in deletion and frame-shift mutagenesis. It has also been reported that DNA bulges play important roles in protein recognition. HMMG-D, a high-mobility group protein, was shown to bind preferentially to bulge sites in DNA (*5*). The binding of the tumor suppression protein p53 to DNA also prefers bulges over other mismatches (*6*).

Our recent work has focused on the design and synthesis of small molecules as specific probes of the role of bulged structures in nucleic acids in various biological processes (*7*, *8*). We have prepared a number of spirocyclic model compounds with specific affinity for bulged sites (two or three unpaired bases) in DNA based on our earlier work with the enediyne antitumor antibiotic neocarzinostatin (NCS-chrom)[1] (*9*−*11*). NCS-chrom undergoes general base-catalyzed activation to a biradical species that selectively cleaves nucleic acids at bulged sites having at least two unpaired bases (*10*−*12*). This reaction was rationalized by a mechanism involving an intramolecular Michael addition, resulting in a spirolactone cumulene intermediate, which further generates a 2,6-didehydroindacene biradical, which

† This research was supported by U.S. Public Health Services Grants GM 53793 to I.H.G. and GM 57123 to G.B.J. from the National Institutes of Health.

The structures have been deposited in the RCSB Protein Data Bank (1P96).

* To whom correspondence should be addressed. Telephone: (617) 432-1787. Fax: (617) 432-0471. E-mail: irving_goldberg@hms.harvard.edu.

‡ Harvard Medical School.

§ Northeastern University.

[1] Abbreviations: 1D, one-dimensional; 2D, two-dimensional; BI, benzindanone; DDI, double-decker intercalator; DG, distance geometry; DQF-COSY, double-quantum-filtered correlation spectroscopy; EDTA, ethylenediaminetetraacetic acid; FID, free induction decay; HPLC, high-performance liquid chromatography; NCS, neocarzinostatin; NCS-chrom, native form of the NCS chromophore; NCSi-gb, postactivated NCS-chrom formed under base-catalyzed conditions; NCSi-glu, post-activated NCS-chrom formed under reductive conditions in the presence of glutathione; NMF, 2-*N*-methylfucosamine; NMR, nuclear magnetic resonance; NA, dihydronaphthone; NAP, dihydronaphthalenone; NPH, hydroxynaphthoate; NOE, nuclear Overhauser effect; NOESY, nuclear Overhauser effect and exchange spectroscopy; rmsd, root-mean-square deviation; THI, tetrahydroindacene; TOCSY, total correlation spectroscopy; TPPI, time-proportional phase incrementation.

10.1021/bi030072d CCC: $25.00
Published on Web 06/21/2003

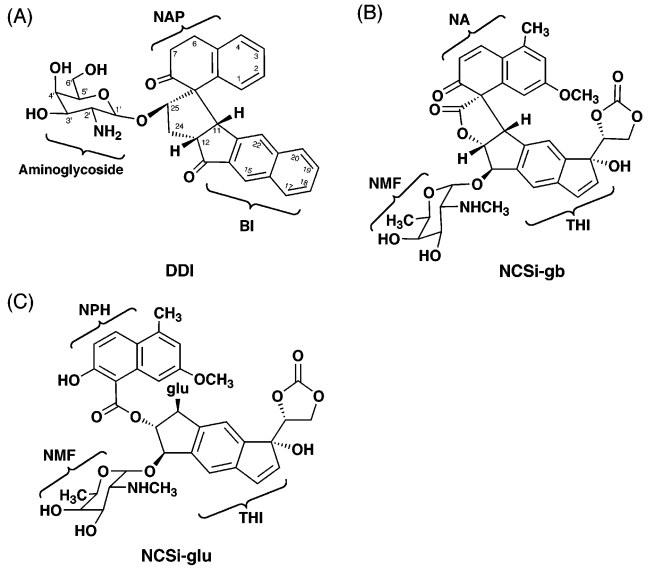

(D)

						G7	T8						
5′−	C1	A2	C3	G4	C5	A6	T9	C10	G11	G12	A13	C14	
3′−	G26	T25	G24	C23	G22	T21	A20	G19	C18	C17	T16	G15	

FIGURE 1: Chemical structures of (A) the synthesized drug (DDI), (B) NCSi-gb, formed under base-catalyzed conditions, (C) NCSi-glu, formed in the presence of glutathione, and (D) the sequence of the bulged DNA duplex consisting of 12-mer nonbulged and 14-mer bulged strands.

is responsible for the hydrogen abstraction from the sugar chain at the bulge site. A detailed mechanistic study of the roles of bulged DNA in the base-catalyzed transformation of NCS-chrom has been reported (*13*). In the absence of a bulged DNA target, a wedge-shaped spirocyclic molecule (NCSi-gb) (Figure 1B) is generated that resembles the DNA cleaving species and binds to the bulged site with great specificity (*14, 15*). On the basis of the solution structure of the complex formed between NCSi-gb and an oligodeoxynucleotide possessing a target bulge site (*16, 17*), we have prepared the wedge-shaped spirocyclic molecule DDI (Figure 1A), whose aglycone structure closely resembles that of the natural product.

DDI mimicks NCSi-gb in having two aromatic ring systems with a right-handed twist angle of 35° imposed by a spirocyclic ring junction. The two ring systems of both molecules are held rigidly at an angle of 60° (as measured by their short axes) by the five-membered spirocyclic ring to form the wedge-shaped molecule. The cyclic carbonate moiety attached to the THI group of NCSi-gb was purposely removed in DDI, since the solution structure of the complex formed by the natural product with DNA containing a two-base bulge showed that it distorts one of the base pairs forming the walls of the binding site (*16, 17*). DDI, which is more stable than the cyclic lactone NCSi-gb, has been shown to bind selectively to bulged DNA and to be a useful probe of the role of bulged structures in DNA strand slippage synthesis. The latter is particularly significant since bulges have been proposed to be involved in the slippage synthesis associated with the unstable expansion of nucleotide repeats in a number of disease conditions, including at least 12 human neurodegenerative diseases (*18*−*21*). These studies have shown that DDI significantly stimulates DNA strand slippage synthesis by DNA polymerase I with a series of primer−template motifs containing different nucleotide repeats (*22*). It seems plausible that DDI binds to or induces the formation of a bulged or related structure that acts as an intermediate in the nucleotide expansion process, and that a derivative of DDI possessing reactive moieties, such as alkylating or cleaving groups, would interfere with this process.

We report here on the elucidation by high-resolution NMR spectroscopy of the structure of the complex formed between DDI and an oligodeoxynucleotide containing a two-base bulge. We show the mode of binding of the synthetic drug, DDI, is different from that of the natural product, NCSi-gb, to the two-base bulged DNA. The structure of the DDI−bulged DNA complex provides a basis for understanding the relative binding affinities of the synthetic agent and the natural product for bulged DNA. These studies provide insights into the nature of the binding reaction and into the design of more effective bulge-binding small molecules.

MATERIALS AND METHODS

Sample Preparation. The synthesis and characterization of DDI have been reported (*8*). DDI was purified by HPLC using a reverse phase C18 column and a gradient of methanol/ammonium acetate buffer. The oligonucleotide sequences, a 14-mer containing a two-base bulge and its complementary 12-mer strand (Figure 1), were synthesized using standard phosphoramidites on an ABI 381A DNA synthesizer. The oligonucleotides were purified by reverse phase HPLC and then desalted with a Sephadex-10 column. The stoichiometry of the duplex formation was verified via titration of the two individual strands above the melting temperature of the duplex, followed by 1D NMR. The resulting two-base bulge DNA duplex was dissolved in a solution containing 0.1 M NaCl, 10 mM sodium phosphate, and 0.1 mM EDTA (pH 6.5). The purity of DDI and DNA oligomers was checked by ^{1}H NMR, and the concentration was measured spectrophotometrically using an ϵ_{260} of 2.436 $\times$ 10^5 M^{-1} cm^{-1} and an ϵ_{253} of 4.12 $\times$ 10^4 M^{-1} cm^{-1}. The 1:1 drug−DNA duplex complex was formed by progressively adding microliter aliquots of a 10 mM stock solution of DDI in d_4-MeOH to the DNA duplex and monitoring the titration by 1D NMR at 25 °C. Formation of the drug−DNA complex was assessed by the disappearance of the resonance lines of the free DNA when DDI was added to the DNA duplex. The complex solution was lyophilized several times and dissolved in 99.96% D_2O. The NMR sample contained a 1:1 DDI−DNA complex at a concentration of ~1.8 mM (pH 6.5).

NMR Experiments. One- and two-dimensional NMR experiments were carried out on Bruker 600 MHz and Varian 500 and 750 MHz spectrometers. Proton chemical shifts were referenced to the HOD resonance (4.7 ppm at 25 °C). ^{31}P chemical shifts were referenced relative to an external trimethyl phosphate in an aqueous solution containing 0.1 M NaCl (pH 6.5).

The inversion recovery pulse sequence (*23*) with τ varied from 3 μs to 1.8 s and a 15.0 s repetition delay was used to estimate T_1 [spin lattice relaxation time, $T_1 \cong \tau_{null}/\ln(2)$, where τ_{null} is the time when the NMR signal intensity is close to zero]. The estimated values of T_1 for aromatic protons of the free DNA and the complex were ~1.2 and ~1.4 s in D_2O, respectively. The inversion recovery experiments were

also used to identify H2 resonances of adenines. These resonances, which exhibit T_1 values longer than those of base and sugar protons, appeared as sharp, negative peaks, while the majority of proton signals were at null intensities.

NOESY, DQF-COSY, TOCSY, and ^{1}H−^{31}P correlation spectra were recorded for the free DNA and the complex in D_2O buffer at 25 °C. NOESY (60, 120, 180, and 250 ms mixing times), DQF-COSY, and TOCSY (30 and 80 ms mixing times) spectra were collected in the phase-sensitive TPPI mode. The spectral width was 6000 Hz, and the pulse delay was 2−4 s. Spectra were acquired using 2048 or 4096 complex points in the t_2 dimension and 512 data points in the t_1 dimension with 32−64 scans per FID. The carrier frequency was placed on the HOD resonance, which was suppressed by presaturation during the relaxation delay. ^{1}H−^{31}P heteronuclear correlation spectra (*24*) were also collected with a spectral width of 2100 Hz in t_2 (^{1}H) and 1200 Hz in t_1 (^{31}P), and 2048 points in the t_2 (^{1}H) dimension and 160 complex points in the t_1 (^{31}P) dimension. Proton NOESY data in H_2O buffer were collected at 1 °C (200 ms mixing time) with the WATERGATE pulse sequence (*25*) for the suppression of the water signal. NMR data were processed using the NMRPipe program (*26*) and analyzed using Sparky version 3.106 (*27*). All NOESY data were apodized by a 90° phase-shifted sine bell function in both dimensions, and DQF-COSY and TOCSY spectra were apodized by a 30° phase-shifted skewed sine bell function. ^{1}H−^{31}P correlation spectra were apodized with a 37.5° phase-shifted skewed sine bell function. All resonances in the free duplex and DDI−DNA complex were assigned using standard procedures (*28*).

NMR Restraints. 2D NOE intensities were determined by the fitting method using a Gaussian function in Sparky version 3.106 (*27*). The interproton distances were derived from the buildup of NOE cross-peak intensities at 60, 120, 180, and 250 ms. Distance ranges of 1.8−2.5, 2.5−3.8, and 3.8−5.5 Å were set for relatively strong, intermediate, and weak NOE cross-peak intensities, respectively. Watson−Crick hydrogen bonding restraints were imposed on the basis of the observed NOEs and chemical shifts of imino protons in the duplex DNA. Standard donor−acceptor atom distances (2.6−3.2 Å) for the hydrogen-bonded atoms in B-DNA were used for all base pairs except the bulge residues. For the two base pairs adjacent to bulge residues, which exhibit a line broadening and upfield chemical shift due to their dynamic flexibility, no hydrogen bonding restraints were applied in the initial stage of the calculation. In the final refinement stage, these hydrogen bonding restraints were applied with lower and upper bounds of ±0.7 Å (±0.35 Å for other base pairs). Additional cross-strand distance restraints (3.0 ± 0.35 Å) were applied for the distances between N3H (dT) and H2 (dA) and between N1H (dG) and N4 (dC), in the base pairs except those adjacent to bulge residues.

Dihedral angle restraints for sugar and backbone torsion angles were obtained from combined analyses of the DQF-COSY and ^{1}H−^{31}P COSY spectra. All of the residues in the DNA duplex except bulge residues were in the C2′-endo family. For these residues, $^3J_{H1'-H2'}$ was greater than $^3J_{H1'-H2''}$ in combination with absent or very weak H2″−H3′ and H3′−H4′ cross-peaks. Therefore, these residues were restrained at a δ of 150 ± 20° (*29*, *30*). No sugar angle restraints were applied in the initial stage of the calculation to the A6, G7, T8, A20, and T21 residues, since most of their COSY cross-peaks were relatively weak in intensity due to line width broadening associated with local motion in the bulge-containing region. The glycosidic torsion angle χ was constrained on the basis of the examination of the H8/H6−H1′/H2′/H3′ distances derived from the 2D NOE spectra (*31*, *32*). The γ angles of all residues except bulge residues were restrained within the *gauche*$^+$ (g^+) conformation (60 ± 20°), since the cross-peaks between H6/H8 and H5′/H5″ protons were weaker than those between H6/H8 and H1′ protons in the short mixing time (60 and 120 ms) NOESY spectra (*30*). The β torsion angles were constrained within the *trans* (*t*) conformation (−150 ± 20°), based on a qualitative interpretation of *J* coupling data using the long-range *n*P−*n*H4′ four-bond coupling. Further restriction of torsion angles β and γ was achieved by the inspection of line widths of the H4′, H5′, and H5″ proton resonances (*29*). The ϵ angle was constrained by the measurement of the heteronuclear $^3J_{H3'-P}$ coupling constants and the observation that no long-range $^4J_{H2'-P}$ was found in the ^{1}H−^{31}P correlation spectrum (*33*). Additionally, the α and ζ torsion angles were restrained on the basis of the observation of the ^{31}P chemical shifts (*34*).

Structure Calculation. A starting model of the two-base bulged DNA duplex was generated in a B-helical conformation using InsightII (Accelrys Inc.). For a starting model of DDI, the aglycone part was built from X-ray coordinates (*8*) and then the aminoglycoside sugar moiety was attached on the spirocyclic alcohol using InsightII. Bad contacts in each molecule were independently removed by conjugate gradient energy minimization without any NMR restraints. The drug was placed more than 8 Å outside the minor groove of the DNA duplex with its orientation relative to the DNA duplex defined by the available intermolecular restraints in the complex.

Structure calculations were performed with distance geometry and simulated annealing protocols within CNS 1.0 (*35*). A large number of initial structures (>200) were generated by distance geometry. These structures were analyzed in terms of the minimum energy, the chirality of sugar protons, and the orientation of the bulge residues. The selected DG structures were subjected to restrained molecular dynamics refinement using the simulated annealing protocol. The structures were heated to 1000 K for 20 ps and then cooled over the course of 25 ps to 300 K. During this calculation, the force constants were 50 kcal mol^{-1} Å^{-2} for experimental distance restraints, 200 kcal mol^{-1} rad^{-2} for dihedral restraints, and 4.0 kcal mol^{-1} Å^{-4} for the van der Waals repulsion term. The structures were refined using 200 steps of restrained energy minimization with NOE and dihedral force constants of 75 kcal mol^{-1} Å^{-2} and 200 kcal mol^{-1} rad^{-2}, respectively. Acceptance criteria of converged structures were low overall energies and no significant NOE (>0.2 Å) or dihedral (>5 Å) violation. Final structures were analyzed using CNS to measure the rmsd between an average structure and the converged structure. Back-calculation of theoretical NMR intensities from the refined structures was performed using CORMA version 5.2 (*36*). The helical parameters of the DNA duplex in the complex were characterized using CURVES version 5.1 (*37*).[2]

[2] Program kindly provided by R. Lavery, CNRS Institut de Biologie Physico-Chimique, Paris, France.

RESULTS

Complex Formation. The dissociation constant (K_d) of DDI complexed with the two-base bulge DNA duplex in 10 mM phosphate buffer (pH 6.5) was determined by fluorescence quenching of the drug upon DNA binding (Figure S1, Supporting Information). The data show that the bulge-containing oligomer binds the drug with a K_d of 2.54 μM, as reported previously (*8*). On the other hand, the binding equilibrium of the complex is slow on the NMR time scale since resonances from free DNA exist as a minor peak in the spectrum of the 1:1 DDI−DNA complex.

The binding of DDI to the two-base bulge-containing DNA duplex (bulged DNA duplex) was monitored by 1D NMR spectroscopy. Figure S2 (Supporting Information) shows one-dimensional ^{1}H NMR spectra of the bulged DNA duplex, both free and in the presence of 1 equiv of DDI, in D_2O buffer at 25 °C. The formation of the DDI−bulged DNA complex is indicated by the changes in the chemical shifts of several residues upon addition of the drug. This is particularly apparent for the methyl protons of thymine and the H8 proton of adenine, which are either bulge residues or adjacent to them. The peaks for A20 H8, T8 CH_3, and T21 CH_3 are downfield-shifted upon complex formation (Figure S2, Supporting Information). DDI−DNA complex formation was also signified by the movements of several imino protons in H_2O buffer at 1 °C (Figure S3, Supporting Information). Upfield shifts for the imino protons of T9, T21, and G19 and a downfield shift for that of G22 were detected upon complex formation, suggesting that DDI binds in the vicinity of the bulge residues of the DNA duplex.

NMR Analysis of DNA in the Complex. The exchangeable proton NMR spectra (10.5−15 ppm) of the free bulge DNA duplex and the DDI−bulged DNA complex in H_2O buffer at 1 °C are shown in Figure S3 (Supporting Information). The imino proton assignments were determined following an analysis of NOE connectivities with nearby protons both across the base pair and to the flanking base pairs in the duplex. The hydrogen-bonded imino protons within base-paired regions resonate between 12 and 14 ppm, whereas the imino protons of the unpaired thymine and guanine at the bulge site resonate between 10 and 11.5 ppm. Twelve base-paired imino protons and two unpaired imino protons were observed in the free duplex and in the complex. An expanded NOESY spectrum recorded in H_2O buffer at 1 °C is shown in Figure 2. The guanine imino protons of the C1G26, C3G24, G4C23, C5G22, C10G19, G11C18, G12C17, and C14G15 base pairs are superpositioned at ∼13.2 ppm, and their assignments were established from the observation of NOEs between the guanine imino protons and cytosine H5 and amino protons. The two thymine imino protons at 13.86 and 13.91 ppm, which exhibit strong NOEs to the adenine H2, are conveniently assigned to T16 and T25, respectively. The remaining two broad imino protons at 12.23 and 12.80 ppm are assigned to T9 and T21, which show observable NOEs to the A20 and A6 adenine H2 pairs, respectively, in the low-contour plot. Such broad and upfield-shifted imino protons of thymine indicate that the A·T base pairs adjacent to the bulge bases experience a fast exchange due to the flexibility of base pairing adjacent to the bulge site (*38*, *39*). The upfield-shifted imino protons at 10−11 ppm are assigned to bulge residues. No NOEs were detected

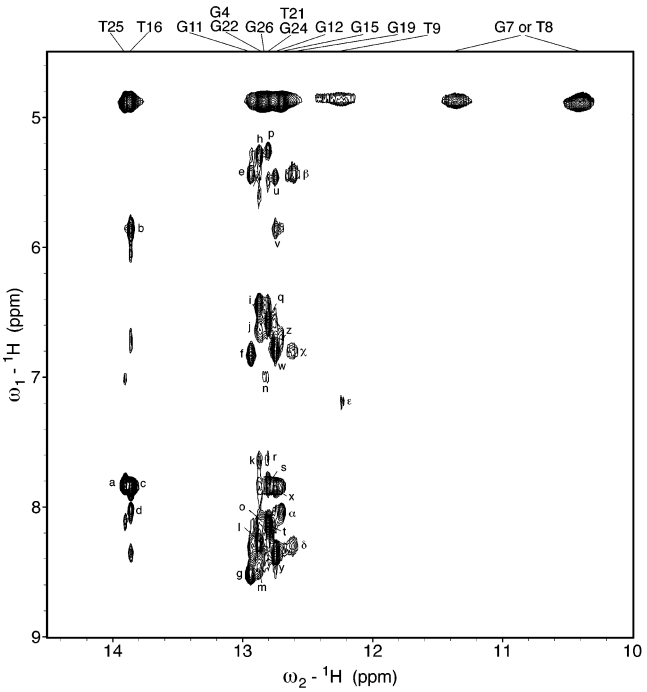

FIGURE 2: Expanded plot of the NOESY (200 ms mixing time) spectrum showing NOE connectivities between the imino protons, and the base and the amino protons for the DDI−bulged DNA complex in H_2O buffer at pH 6.5 and 1 °C. Assignments of the imino protons are labeled at the top of the spectrum. Peaks labeled a−z and α−ϵ are assigned as follows: (a) A2 H2−T25 NH, (b) A13 NH_2[e]−T16 NH, (c) A13 H2−T16 NH, (d) A13 NH_2[b]−T16 NH, (e) C18 H5−G11 NH, (f) C18 NH_2[e]−G11 NH, (g) C18 NH_2[b]−G11 NH, (h) C23 H5−G4 NH, (i) C23 NH_2[e]−G4 NH, (j) C5 NH_2[e]−G22 NH, (k) A6 H2−G22 NH, (l) C23 NH_2[b]−G4 NH, (m) C5 NH_2[b]−G22 NH, (n) C1 NH_2[e]−G26 NH, (o) C1 NH_2[b]−G26 NH, (p) C3 H5−G24 NH, (q) C3 NH_2[e]−G24 NH, (r) A6 H2−T21 NH, (s) A2 H2−G24 NH, (t) C3 NH_2[b]−G24 NH, (u) C17 H5−G12 NH, (v) A13 NH_2[b]−G12 NH, (w) C17 NH_2[e]−G12 NH, (x) A13 H2−G12 NH, (y) C17 NH_2[b]−G12 NH, (z) C14 NH_2[e]−G15 NH, (α) C14 NH_2[b]−G15 NH, (β) C10 H5−G19 NH, (χ) C10 NH_2[e]−G19 NH, (δ) C10 NH_2-[b]−G19 NH, and (ϵ) A20 H2−T9 NH. The symbols b and e refer to the hydrogen-bonded and exposed cytosine amino protons, respectively, involved in Watson−Crick base paring.

between the imino proton of the bulge residues and other amino and nonexchangeable protons in the NOESY contour plots of the complex due to a rapid exchange with solvent. The upfield shifts of the resonance on complex formation were observed for the imino protons of T9 (−0.13), T21 (−0.14), and G19 (−0.08) and amino protons of C10 (−0.07 and −0.07 for bound and nonbound protons, respectively), and downfield shifts were observed for the imino proton of G22 (0.12) and the amino protons of C5 (0.12 and 0.09 for bound and nonbound protons, respectively), indicating that a preferential binding site is near the bulge region. The chemical shifts of the exchangeable protons are listed in Table S1 of the Supporting Information.

Nonexchangeable proton assignments were based on an analysis of the NOESY data set (70 and 250 ms mixing times) and TOCSY (80 ms spin lock time) and DQF-COSY at 25 °C. The expanded NOESY (250 ms mixing time) contour plot establishing sequential connectivities between the base protons (7.0−8.4 ppm) and the sugar H1′ and cytosine H5 protons (5.0−6.5 ppm) of the DDI−bulged DNA complex is given in Figure 3. The base to sugar H1′ proton

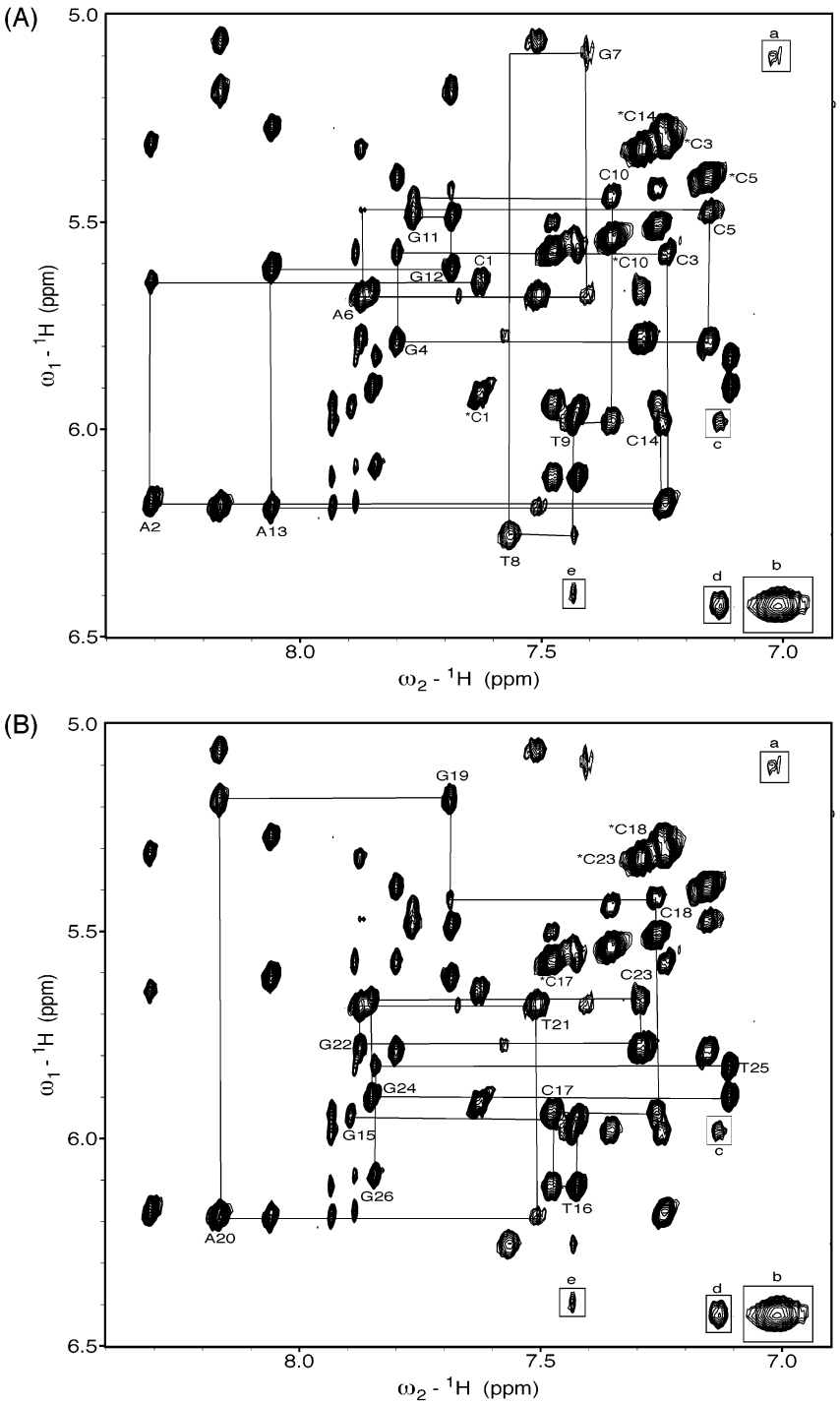

FIGURE 3: Expanded plot of the NOESY (250 ms mixing time) spectrum of the DDI−bulged DNA complex in D_2O buffer at pH 6.5 and 25 °C. The solid lines indicate the H1′−H6/H8 sequential connectivities observed along the duplex. (A) Sequential NOE connectivities for the bulge-containing strand of C1−C14. (B) Sequential NOE connectivities for the complementary strand of G15−G26. Asterisks denote cytosine H6−H5 cross-peaks. The intermolecular NOEs between the DDI and DNA protons and the intramolecular NOEs between DDI protons are shown in boxes. The labels correspond to NOEs between the following protons: (a) DDI H3−G7 H1′, (b) DDI H2−DDI H3, (c) DDI H4−T9 H1′, (d) DDI H2−DDI H4, and (e) DDI H20−T9 H6.

connectivities are traced from C1 to C14 along the bulge-containing strand (Figure 3A) and from G15 to G26 along the complementary strand (Figure 3B). The overall pattern of NOE cross-peaks and relative intensities is consistent with a right-handed double helix and a glycoside torsion angle in the anti range for the complex. A weak NOE cross-peak between C5 H1′ and A6 H8 was observed. The NOE cross-peak between A6 H1′ and G7 H6 was weak due to an overall line broadening of the G7 protons, but its intensity was as strong as that of the intraresidue NOE. The interruption in the connectivities was detected at the G7-T8 step, which are bulge residues. Also, a weak NOE cross-peak was observed between T8 H1′ and T9 H6. Moreover, the H8−H2′/H2″ sequential NOE peaks for the G7-T8 and T8-T9 steps were absent or weak, whereas the H8−H2′/H2″ sequential NOE peaks for the C5-A6 and A6-G7 steps were clearly observed (Figure S4, Supporting Information). In addition, unusually strong NOE peaks were detected for G7 H3′−T8 H6, G7

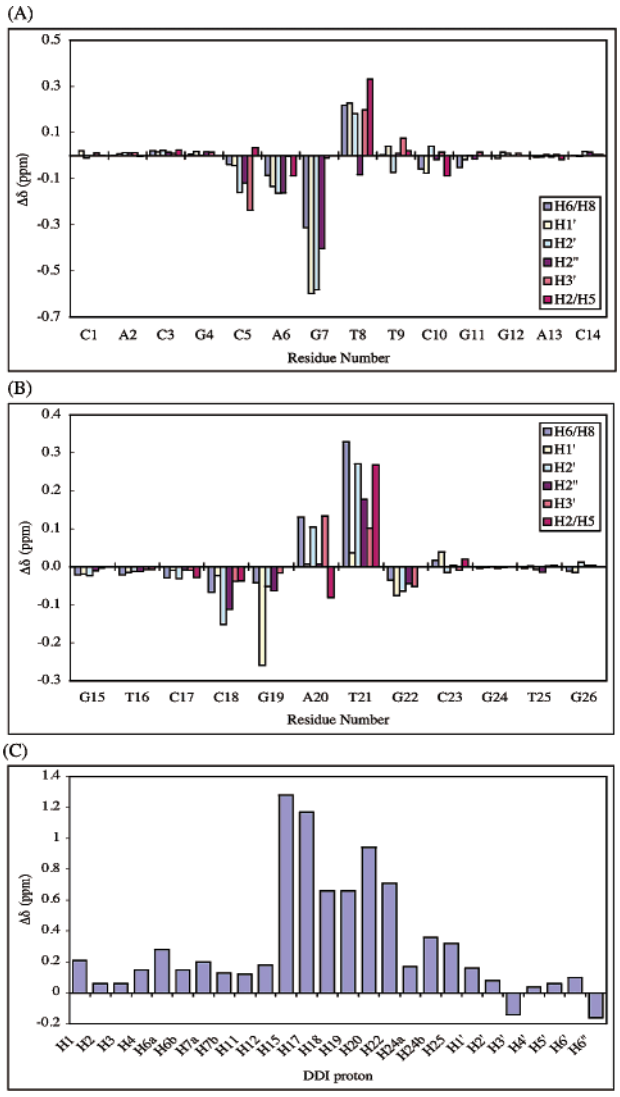

FIGURE 4: Chemical shift changes for oligonucleotides of the DDI−bulged DNA complex relative to the free DNA duplex and bound DDI relative to the free DDI. Negative values of $\Delta\delta$ represent upfield chemical shift changes. (A) DNA residues in the bulge-containing strand. (B) DNA residues in the complementary strand. (C) DDI.

H3′−T8 CH_3, and T8 H1′−T9 CH_3 cross-peaks. These data indicate that one of the unpaired bases, G7, stacks inside the helix, whereas the other one, T8, is localized at an extrahelical position. In the complementary strand, T21 H6 exhibited a weak sequential NOE cross-peak to A20 H1′, and T21 CH_3 exhibited an unusually strong NOE cross-peak to A20 H3′. Numerous changes in chemical shift are observed for the nonexchangeable protons in the DDI−bulged DNA complex, relative to the free bulge DNA duplex (Figure 4A,B). Upfield chemical sifts are observed for the H2′, H2″, and H3′ protons of C5, the H1′, H2′, and H2″ protons of A6, and the H6, H1′, H2′, and H2″ protons of G7 in the bulge-containing strand and for the H2′ and H2″ protons of C18, the H1′ proton of G19, and the H2 proton of A20 in the complementary strand. Further, significant downfield shifts are observed for protons of T8, A20, and T21 upon complex formation. These perturbations were localized near the bulge site. The resonances of C5, A6, G7, and T8 of the bulge-containing strand and C18, G19, A20, and T21 of the complementary strand exhibit modest to large chemical shift changes upon complex formation. It has to be noted that the resonances associated with the G7 residue are especially broad and the most upfield shifted upon complex formation, an indication of the conformational change of G7 upon drug binding. The chemical shifts of the nonexchangeable protons are listed in Table S2 of the Supporting Information.

The proton-decoupled phosphorus spectrum of the complex has been recorded in D_2O buffer at pH 6.5 and 25 °C. The phosphorus resonances are dispersed over a 1.3 ppm range between −3.2 and −4.5 ppm. The phosphorus resonances have been assigned from an analysis of the proton-detected phosphorus−proton heteronuclear correlation experiment with the expanded contour plot shown in Figure S5 (Supporting Information). The most upfield ^{31}P resonances at −4.28 and −4.37 ppm are assigned to T8 and A20, respectively, and the most downfield ^{31}P resonance at −3.40 ppm is assigned to C10. The phosphorus resonances for the free DNA duplex and the complex and their chemical shift difference are given in Table S3 of the Supporting Information. The ^{31}P resonances of A6, T8, and A20 are upfield-shifted and the ^{31}P resonances of C10 and T21 downfield-shifted upon complex formation. Since ^{31}P chemical shifts are sensitive to bond and torsion angles connecting P to coordination atoms, the significant shifts of ^{31}P resonances upon complex formation are strong evidence that the backbone conformation of the complex is different from that of the free duplex. This perturbation in ^{31}P chemical shifts is in accord with chemical shift changes of proton resonances on complex formation.

NMR Analysis of DDI in the Complex. The NMR spectra of free DDI in CD_3OD were previously characterized for complete chemical shift assignment and structural conformation. All proton resonances of DNA-bound DDI were assigned in a manner similar to that described for the assignments of the free DDI (*8*). The chemical shifts for DDI, both free in an aqueous solution and when bound to the bulge DNA duplex, are shown in Table S4 of the Supporting Information. Proton resonances of DDI in the complex were restricted to only one set, exhibiting spin connectivities and characteristic intramolecular NOEs similar to those of the free DDI. DDI in the bound form also exhibits a strong H25−H1 NOE cross-peak and medium H11−H6 and H22−H6 NOE cross-peaks, which are characteristic NOEs between aglycone protons, and a strong H1′−H25 NOE cross-peak and weak H1′−H24a and H5′/H6′/H6″−H1 NOE cross-peaks, which are interesidue NOEs between aglycone and aminoglycoside protons. Also, aminoglycoside sugar H1′ is scalar coupled to H2′ and shows strong NOE cross-peaks to H3′ and H5′, indicating that the chair form of the glycoside sugar remains unchanged upon complex formation. Several NOEs between DDI protons in the complex are shown in Figure 5, and all of the characteristic intramolecular NOEs of DDI are listed in Table S5 of the Supporting Information.

The resonances of the BI ring protons in the complex exhibit the most significant upfield shift (0.66−1.18 ppm) compared to that of free DDI. These large upfield-shifted resonances in the bound DDI are an indication of intercalation by the BI upon complex formation. On the other hand, the resonances in the NAP and aminoglycoside moieties are mostly upfield shifted with smaller changes compared to the

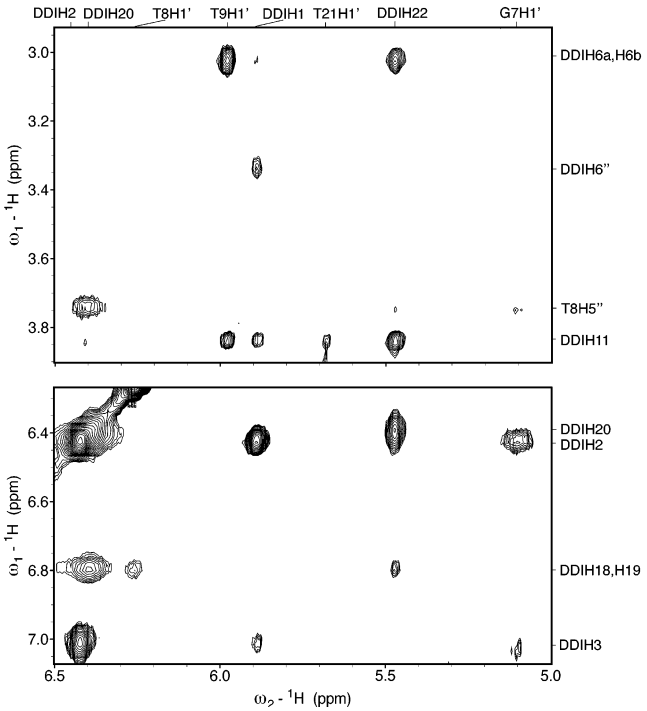

FIGURE 5: Expanded region of the NOESY spectrum showing the intramolecular and intermolecular cross-peaks of DDI. Assignments of peaks are shown at the top and right side of the spectrum.

BI moiety. The chemical shift differences of DDI between the free and complexed forms are shown in Figure 4C.

Intermolecular NOEs in the Complex. A number of intermolecular NOEs between the bulged DNA duplex and DDI protons have been identified and assigned for the DDI−bulged DNA complex. Several intermolecular NOEs are shown in Figure 5 and in an expanded NOESY contour plot of the nonexchangeable protons (Figure 3 and Figure S4A).

The largest number of intermolecular NOEs are identified between the two aromatic ring protons of DDI, BI and NAP, and the G7-T8-T9 sequence of the bulge-containing strand, indicating that the two aromatic rings of DDI are positioned toward the bulge region. It is readily apparent that most of components of the DDI, except the intercalated BI ring system, show extensive NOEs to primarily the DNA minor groove protons (*40*). These intermolecular NOEs are listed by residue position within each component of the complex in Table 1 and provide critical restraints for aligning the DDI on the DNA and defining the solution structure the complex.

The distribution of the observed intermolecular NOEs readily provides insights into the alignment of the intercalated BI ring system at the bulge site. The H18, H19, and H20 protons of BI moiety show NOEs to the base and methyl protons of T8 and T9 and sugar protons of G7, T8, and T9 (Table 1). Also, the H11 proton of the other short edge of the BI moiety shows NOEs to the H2 proton of A20 and the H1′ proton of T9. These NOE patterns suggest that the BI moiety is intercalated at the bulge pocket formed by the G7-T8-T9·A20 sequence and positioned toward the major groove. The NAP moiety, the other ring system of DDI, exhibits several NOEs to minor groove protons (H1′ and H4′) of G7, T8, and T9 of the bulge-containing strand, establishing that the NAP moiety is positioned in the minor groove of the bulge site. The aminoglycoside sugar ring is also positioned in the minor groove on the basis of the observed

Table 1: Intermolecular NOEs Observed between DDI and DNA Protons

DDI	DNA contacts
H1	G7 H1′
H2	G7 H1′, G7 H2″, G7 H4′, T8 H5″
H3	G7 H1′, G7 H2″, T8 H4′, T8 H5′, T8 H5″
H4	T8 H4′, T8 H5″, T9 H4′, T9 H5′, T9 H5″
H6a, H6b	T9 H1′, T9 H2″, T9 H4′
H11	T9 H1′, A20 H2
H18	T9 CH_3
H19	G7 H1′, G7 H2′, G7 H2″, T8 H1′, H8 H4′, T8 H5′, T8 CH_3, T9 CH_3, T9 H6
H20	G7 H1′, G7 H2″, T8 H1′, T8 H4′, T8 H5′, T8 H5″, T9 CH_3, T9 H6
H22	T8 H4′, T8 H5′, T9 H1′, T9 H4′
H24a, 24b	T21 H4′, T21 H5′, T21 H5″
H5′	A6 H2
H6′, H6″	A6 H2

NOEs between H5′, H6′, and H6″ of the aminoglycoside and the H2 proton of A6. Additionally, H24a and H24b protons of the spirocyclic ring, which connects the two ring systems and the aminoglycoside, exhibit NOEs to H4′ and H5″ of T21, providing evidence for DNA bulge binding from the minor groove. Thus, all of the intermolecular NOEs suggest that the BI moiety is intercalated toward the bulge pocket formed by the G7-T8-T9·A20 sequence, while the NAP and aminoglycoside moieties remain in the minor groove at the site of the bulge pocket and adjacent to the A6·T21 base pair, respectively.

Sugar Conformation. The H1′−H2′ cross-peaks in the DQF-COSY spectrum indicate that all nonterminal residues are in the C2′-endo sugar conformation domain except the bulge residues (G7 and T8), for which it is impossible to extract *J* coupling and intensity data due to a spectral overlap and line broadening. The $^2J_{H1'-H2'}$ coupling constants were found to vary between 8.8 and 11.5 Hz. Further, the H2″−H3′ cross-peaks are absent for all nonterminal residues except bulge residues. For the sugars of the terminal and bulge residues, which presumably exhibit a more complex dynamic behavior caused by end fraying and flexible motion, no sugar torsion angle constraints were applied.

Structure Calculation. A set of 554 intra-DNA distances were derived from nonexchangeable ^{1}H NOE volumes and consisted of 367 intranucleotide restraints and 187 internucleotide restraints. Forty-seven DNA−drug intermolecular NOEs provide information about the binding site of the drug. These NMR results were incorporated as initial distance and dihedral angle restraints in the structure calculation. The structure computation was carried out in an iterative manner in which distances derived from the calculated structures were compared with the experimental data. On the basis of these analyses, distance bounds and NOE force constants of various groups of NOE restraints were adjusted, and a new generation of structures was calculated using the newly modified protocol. The final structures were selected on the basis of criteria such as low overall energies and no significant NOE (>0.2 Å) and dihedral (>5 Å) violation. Ten superimposed structures are presented as the final results in Figure 6. The final refined structures converged to a pairwise rms difference of 0.89 and an average rms difference of 0.62, and very low constraint violation energies (Table 2). These converged structures show good bond and angle

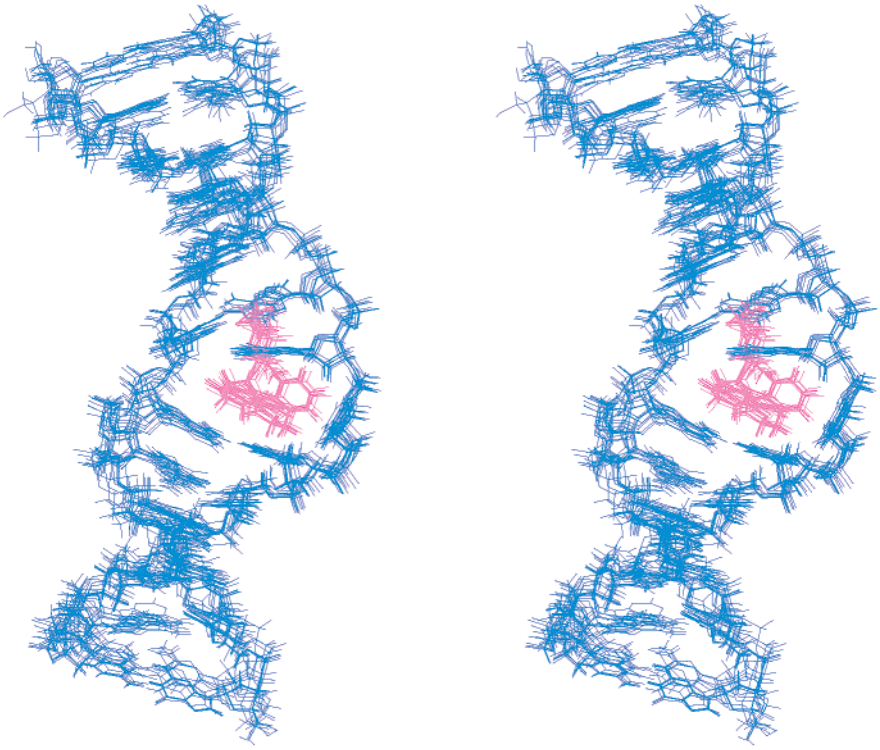

FIGURE 6: Stereoview of the superimposed final 10 refined structures as determined by simulated annealing for the DDI−bulged DNA complex viewed from the minor groove. The DNA and drug are shown in blue and pink, respectively.

Table 2: Structural Statistics of the 10 Refined Structures of the DDI−Bulged DNA Complex

no. of NOE distance restraints	694
intraresidue (DNA)	367
interesidue (DNA)	187
hydrogen bond (DNA)	32
intraresidue (DDI)	43
intermolecular (DDI−DNA)	47
no. of torsion angle restraints	166
no. of distance violations >0.20 Å	0
rmsd of distance violations (Å)	0.0290 ± 0.0002
no. of dihedral angle violations >5°	0
rmsd of dihedral angle violations (deg)	0.2187 ± 0.0099
rmsd for ideal bond lengths (Å)	0.0036 ± 0.00007
rmsd for ideal bond angles (deg)	0.4807 ± 0.0075
rmsd for ideal impropers (deg)	0.4306 ± 0.0005
pairwise rmsd (Å)	0.894 ± 0.4038
rmsd relative to the averaged structure (Å)	0.627 ± 0.2303

geometry and in general satisfy NMR-derived distances and dihedral angles.

The accuracy of the calculated structures was judged by complete relaxation matrix analysis using CORMA. The theoretical NOE spectrum was predicted from the average structure of refined DDI−bulged DNA complexes, and an expanded NOESY region between the base proton and the sugar H2′ and H2″ protons is displayed in Figure S4B of the Supporting Information. These data show that the theoretical intraresidue and interresidue NOEs for the refined structure of the DDI−DNA complex are in accord with experimental NOEs, suggesting reasonable agreement between the refined structure and the NOE data.

Elucidation of the Structure of the DDI−Bulged DNA Complex. The BI moiety is intercalated into the helix from the minor groove, while the NAP and aminoglycoside moieties are positioned in the minor groove. Space-filling

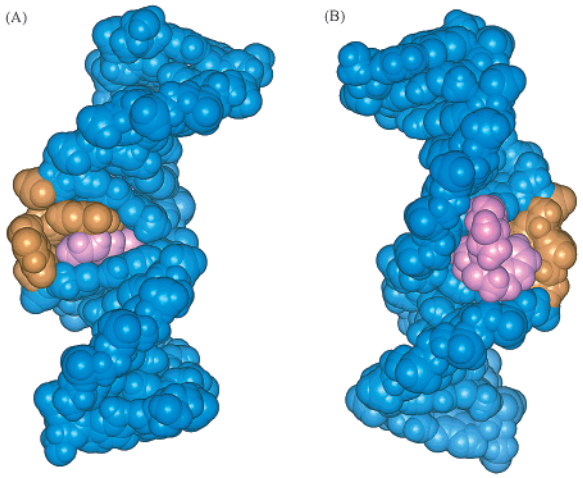

FIGURE 7: Two space-filling views looking into (A) the major groove and (B) the minor groove of the DDI−bulged DNA complex. The DNA and drug are shown in blue and pink, respectively. The two bulge residues are shown in orange.

views of the averaged structure of the DDI−bulged DNA complex that differ by a 90° rotation along the helix axis are shown in Figure 7. These views emphasize that intercalation of the BI ring system is toward the bulge pocket of the major groove (Figure 7A), that the aminoglycoside ring is in the middle of the minor groove, and that the NAP ring is placed into the bulge site of the minor groove (Figure 7B). Intercalation of the BI moiety between G7 and the T9·A20 base pair in the complex is shown in Figure 8A as a view normal to the helix. The approach of the NAP moiety toward the bulge region of the minor groove and the positioning of sugar ring within the wall of the minor groove in the DDI−bulged DNA complex are shown in Figure 8B.

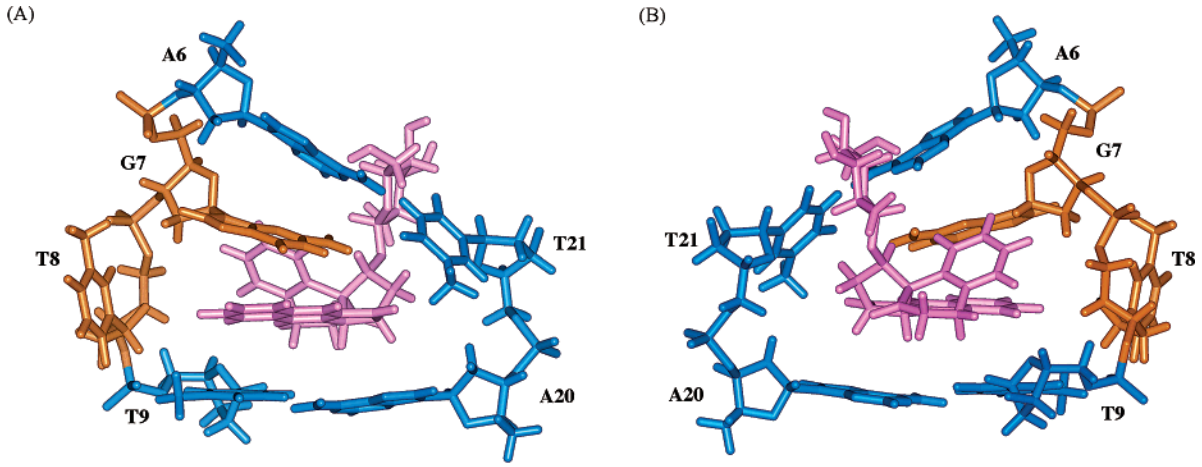

FIGURE 8: Stick view of the binding site in the DDI−bulged DNA complex looking into the major (A) and minor (B) groove. The color code is the same as outlined in the legend of Figure 7. The A6·T21 and T9·A20 base pairs are shown in blue.

DISCUSSION

Complex Formation and Bulge Specificity. Fluorescence quenching studies have identified a two-base bulge in otherwise duplex DNA as the preferred binding site for both DDI and NCSi-gb (*8*, *15*). The overall specificity and tightness of binding to two-base bulge-containing oligonucleotides are ~10-fold greater for the natural product. In each case, high-resolution NMR reveals a unique structure of the drug−DNA complex, with drug binding limited to the bulge site.

Global Structural Features of the DDI−Bulged DNA Complex. The BI moiety of DDI intercalates by way of the minor groove into the G7-T8-T9·A20 pocket, consisting of a helical base pair and two unpaired bulge bases. The spirocyclic ring with its attached aminoglycoside is positioned in the minor groove aligning along the A20-T21-G22 sequence of the nonbulged strand, while the NAP moiety, its position restrained by the spirocyclic ring, aligns in the minor groove mainly along the G7-T8-T9 bulge-containing strand. The BI ring system stacks diagonally with respect to the T9·A20 base pair, overlapping with part of the purine base A20 and minimally with the six-membered ring of G7. In accordance with the NOE interactions described above, the distal edge of the BI aromatic ring system protrudes into the major groove near the G7-G8-T9 bulge pocket, whereas the other end of the ring is located above the H2 proton of the A20 residue. The proton most upfield-shifted by DDI binding, H1′ of G7, presumably located above the aromatic ring system of BI, is strongly affected by the ring current of the aromatic ring system of DDI (*41*). The same is true for the protons of the BI ring system, which are the only drug protons directly above or below the DNA bases. Most of protons of the BI ring system are strongly upfield-shifted due to the ring current of the bases, whereas the other protons of the NAP and aminoglycoside moieties bound in the minor groove are shifted modestly upfield compared to those of the BI ring system. It should be emphasized that the BI moiety, stacking between the T9·A20 base pair and bulge residue G7, behaves partially as a pseudobase inside the duplex DNA, providing additional stacking continuity, which releases the stress in the DNA backbone caused by bending of the helical axis. The DDI−bulged DNA complex is likely stabilized by the stacking interactions between the aromatic moieties in the bulge intercalation site and the van der Waals interactions between DDI and the DNA along the minor groove.

DNA Structure in the Complex. The bulged DNA duplex adopts a right-handed helix with 12 Watson−Crick base pairs in the DDI−DNA complex. However, NMR data show that two A·T base pairs adjacent to the bulge residues are weaker than regular base pairs due to the flexibility of the bulge segment (*38*, *39*). In particular, the A6·T21 base pair is partially distorted as compared to the other base pairs, due to the close approach of the aminoglycoside sugar moiety in the minor groove. The glycoside torsion angles are all in the anti range, and the sugar pucker geometries are C2′-endo except for those of the two bulge bases (Table S6, Supporting Information). Pronounced helical unwinding was observed near the bulge site in the complex. The minor groove widens at the binding site around the bulge residues to provide room for accommodation of the rigid spirocyclic structure consisting of three moieties. The bend around the bulge binding site as represented by the central axis of the oligodeoxynucleotide is ~42°, very similar to that reported for NCSi-gb (*16*). Also, with both agents the 3′-flanking strand of the bulge site is more bent than the 5′-flanking strand.

The NMR-derived refined structure shows that the location and role of each of the two bulge residues at the binding site are different upon complex formation. The unpaired purine base G7 is intrahelical, stacking between the A6 residue of DNA and the intercalated aromatic moiety (BI ring system) of DDI. The stacking of the G7 residue is clearly shown by the presence of sequential NOE connectivities between H1′, H2′, and H2″ of A6 and H8 of G7 and NOEs between H1′ of G7 and H19 and H20 of DDI. In contrast, the unpaired pyrimidine base T8 is extrahelical, providing the third binding surface at the bulge binding site upon complex formation. These placements of two bulge bases are consistent with the previous structural studies of bulge-containing duplexes, where the purine and pyrimidine bases prefer to stack into or loop out of the DNA helix, respectively, depending on their flanking sequences and temperature (*38*, *42*, *43*). Indeed, placement of the bulge bases at the bulge binding site of the DDI−bulge DNA complex differs from that of the two unpaired bases of the NCSi-gb−bulged DNA complex, both of which are extrahelical, thus permit-

ting insertion of the two aromatic moieties into the bulge pocket. Contrary to the situation with NCSi-gb, the aminoglycoside moiety of DDI blocks the intercalation of the NAP moiety into the bulge site so that it remains in the minor grove of the DNA helix. One of the bulge bases, G7, stacks at the bulge binding site, providing a stacking connectivity in the duplex.

Comparison with Complexes of the Postactivated Neocarzinostatin Chromophore with Bulged DNA. Thiol activation of NCS-chrom generates a radical species with specificity for cleavage near a single-base bulge (*45*−*47*), whereas general base-catalyzed intramolecular activation of the drug leads to a radical species with great specificity for a two-base bulge (*11*). The solution structures of the complexes formed between the NCS-chrom postactivated species (NCSi-glu and NCSi-gb, Figure 1) and their bulge targets have been elucidated and reveal remarkably different binding modes (*16*, *17*, *48*). In the complex formed by NCSi-gb and an oligonucleotide with a two-base bulge, the wedge-shaped drug product fits snugly into a triangular prism binding cavity, consisting of the two helical base pairs on either side of the bulge and the two bulged out bases (*16*, *17*). The two ring systems of the drug are fixed relative to each other and have a right-handed twist of ∼35°. Unlike most aminoglycosides, the NMF moiety of NCSi-gb recognizes the major groove and acts as an anchor, determining the depth to which the drug can penetrate into the major groove. In the binding cavity, the NA and the THI moieties, connected through a spirolactone, are mimics of helical DNA bases, complementing the bent DNA structure, and stack with the base pairs above and below. On the other hand, the complex formed by NCSi-glu with its target single-base bulged DNA occurs by way of the minor groove (*48*). The NPH moiety of NCSi-glu intercalates into the bulge site, and its substituent groups, the NMF carbohydrate ring and the THI, form a complementary minor groove binding surface. In this structure, the glutathione tripeptide contributes to the stability of the bulge site by being partially embedded within it and pushes the THI toward the opposite strand, where the radical species of the drug induces oxidative strand cleavage at the 3′-side, opposite from the bulge.

The aglycone structure of DDI can almost be superimposed on that of NCSi-gb (*8*), but its binding mode shares features with that of both NCSi-gb and NCSi-glu. Binding of DDI is through the minor groove, and only one aromatic planar ring system intercalates into the bulge site, positioning all the other parts in the minor groove. Whereas the NPH moiety, the two-ring system of NCSi-glu, intercalates at the bulge binding site, it is the BI moiety, the three-ring system of DDI, that intercalates at the bulge pocket. Further, the THI moiety, the other ring system of NCSi-glu, aligns mainly along the strand opposite the bulge site (consistent with the cleavage data), whereas the NAP moiety of DDI is near the bulge pocket. Despite the striking similarity of the geometries of their aglycone structures, DDI binds via the minor groove and NCSi-gb by way of the major groove. This difference in binding mode can be attributed to the difference in the attachment sites of their pendant aminoglycoside moieties (Figure 1). Also, whereas both aromatic ring moieties of NCSi-gb insert into the triangular prism binding pocket formed by the two looped out bulge bases and the neighboring base pairs, only one aromatic ring of DDI intercalates into the bulge pocket. However, unlike NCSi-glu, both aromatic ring moieties of NCSi-gb and DDI are located in the bulge site, presumably because of the common spirocyclic structure. This difference in binding mode between the two molecules likely accounts for the previously observed lower specificity and tightness of binding of DDI for the two-base bulge site (*8*).

Bulge Recognition by the Synthesized Drug and Implications for Drug Design. We have synthesized DDI as a bulge target binding molecule by mimicking the wedge-shaped spirocyclic aglycone of NCSi-gb. As noted above, although DDI binds to the bulge binding site in a specific manner, the minor groove binding pattern of DDI contrasts with the major groove interaction of NCSi-gb, and this difference has been attributed to the difference in aminoglycoside placement. In their respective NMR-derived complexes with bulged DNA, the sugar moiety of NCSi-gb, which is attached to THI, extends away from the aglycon, whereas the aminoglycoside moiety of DDI, which is attached to the spirocyclic five-membered ring, aligns closely (at an angle of ∼60°) with the NAP ring system as shown by the intramolecular NOEs (Table S5, Supporting Information). Therefore, intercalation of the NAP moiety into the bulge binding site is precluded by the aminoglycoside moiety. Indeed, the A6·T21 base pair is significantly distorted in the DDI-bulged DNA complex by the approaching aminoglycoside moiety. Only the BI ring system, which extends away from the aminoglycoside, is able to intercalate into the bulge pocket. Although the NAP moiety remains in the minor groove at the bulge site instead of intercalating into the bulge pocket, it provides additional van der Waals stabilization through the interaction with sugar protons of both bulge residues comprising the bulge pocket, as shown by the intermolecular NOEs in Table 1. On the basis of this structural study, spirocyclic derivatives with the aminoglycoside attached to the same position on the aglycone as in the natural product are being synthesized in an effort to overcome the positional hindrance of this moiety on the intercalative binding of both ring systems of the drug. Such compounds would be expected to resemble the natural product more closely in their bulge binding characteristics and in their ability to modulate DNA strand slippage synthesis.

Elucidation of the structure of the DDI−bulged (two-base) DNA complex provides a basis for understanding the relative binding affinities of the synthetic agent and NCSi-gb for bulges of different sizes. NCSi-gb and DDI bind to a two-base bulge-containing oligodeoxynucleotide with 1000- and 4-fold greater affinities, respectively, than to one with a single-base bulge (*8*), whereas NCSi-glu binds equally well to both substrates (although cleavage is much better at the one-base bulge site) (*46*). The inability to insert both ring systems of DDI into the bulge site results in G7 remaining in an intrahelical position and culminates in less stable binding for the synthetic agent.

ACKNOWLEDGMENT

We appreciate the availability of NMR time provided at the Harvard Medical School. We thank X. Gao (University of Houston, Houston, TX) for suggesting the binding mode and for allowing us to use the NMR facility funded by the

W. M. Keck Foundation in our initial experiments. We also thank Dr. X. Gao and Y. Kwon for critical reading of the manuscript and the latter for help in use of the NMR facility. We thank F. S. Fouad and Z. Xi for the chemical synthesis of DDI and J. Lee for help in using the CNS program.

SUPPORTING INFORMATION AVAILABLE

Chemical shift assignments for the exchangeable protons (Table S1) and the nonexchangeable protons (Table S2), chemical shift assignments of the phosphorus resonances and their differences for the bulged DNA in the complex and in the free form (Table S3), ^{1}H NMR chemical shifts of DDI in the free and complex form (Table S4), intramolecular NOEs observed between DDI protons (Table S5), helical parameters of the DNA in the DDI−bulged DNA complex (Table S6), fluorescence quenching of DDI by the bulged DNA duplex (Figure S1), ^{1}H NMR spectra of the free bulged DNA duplex (Figure S2A) and the 1:1 DDI−bulged DNA duplex complex (Figure S2B), imino proton spectra of free bulged DNA duplex (Figure S3A) and the 1:1 DDI−bulged DNA duplex complex (Figure S3B), expanded NOESY contour plot of the base to H2′/H2″ region for the DDI−bulged DNA complex (Figure S4A), back-calculation spectrum of the refined structure of the DDI−bulged DNA complex showing NOEs between the base and sugar H2′/H2″ protons (Figure S4B), and the contour plot of the proton-detected ^{1}H−^{31}P correlation spectrum of the DDI−bulged DNA complex (Figure S5). This material is available free of charge via the Internet at http://pubs.acs.org.

REFERENCES

1. Turner, D. H. (1992) Bulges in nucleic acids, *Curr. Opin. Struct. Biol. 2*, 334−337.
2. Lilley, D. M. J. (1995) Kinking of DNA and RNA by base bulges, *Proc. Natl. Acad. Sci. U.S.A. 92*, 7140−7142.
3. Chastain, M., and Tinoco, I. (1991) Structural elements in RNA, in *Progress in Nucleic Acid Research and Molecular Biology* (Cohn, W. E., and Moldave, K., Eds.) Vol. 41, pp 131−177, Academic Press, New York.
4. Kunkel, T. A. (1993) Slippery DNA and diseases, *Nature 365*, 207−209.
5. Payet, D., Hillisch, A., Lowe, N., Diekmann, S., and Travers, A. (1999) The recognition of distorted DNA structures by HMG-D: a footprinting and molecular modelling study, *J. Mol. Biol. 294*, 79−91.
6. Degtyareva, N., Subramanian, D., and Griffith, J. D. (2001) Analysis of the binding of p53 to DNAs containing mismatched and bulged bases, *J. Biol. Chem. 276*, 8778−8784.
7. Xi, Z., Jones, G. B., Qabaja, G., Wright, J. W., Johnson, F. S., and Goldberg, I. H. (1999) Synthesis and DNA binding of spirocyclic model compounds related to the neocarzinostatin chromophore, *Org. Lett. 1*, 1375−1377.
8. Xi, Z., Hwang, G.-S., Goldberg, I. H., Harris, J. L., Pennington, W. T., Fouad, F. S., Qabaja, G., Wright, J. M., and Jones, G. B. (2002) Targeting DNA bulged microenvironments with synthetic agents: Lessons from a natural product, *Chem. Biol. 9*, 925−931.
9. Xi, Z., and Goldberg, I. H. (1999) DNA-Damaging Enediyne Compounds, in *Comprehensive Natural Products Chemistry* (Barton, D. H. R., Nakanishi, K., and Meth-Cohn, O., Eds.) Vol. 7, pp 553−592, Elsevier Science, Oxford, U.K.
10. Kappen, L. S., and Goldberg, I. H. (1993) DNA conformation-induced activation of an enediyne for site-specific cleavage, *Science 261*, 1319−1321.
11. Kappen, L. S., and Goldberg, I. H. (1993) Site-specific cleavage at a DNA bulge by neocarzinostatin chromophore via a novel mechanism, *Biochemistry 32*, 13138−13145.
12. Kappen, L. S., and Goldberg, I. H. (1995) Bulge-specific cleavage in transactivation response region RNA and its DNA analogue by neocarzinostatin chromophore, *Biochemistry 34*, 5997−6002.
13. Xi, Z., Mao, Q. K., and Goldberg, I. H. (1999) Mechanistic studies on the base-catalyzed transformation of neocarzinostatin chromophore: Roles of bulged DNA, *Biochemistry 38*, 4342−4354.
14. Hensens, O. D., Chin, D.-H., Stassinopoulos, A., Zink, D. L., Kappen, L. S., and Goldberg, I. H. (1994) Spontaneous generation of a biradical species of neocarzinostatin chromophore: role in DNA bulge-specific cleavage, *Proc. Natl. Acad. Sci. U.S.A. 91*, 4534−4538.
15. Yang, C. F., Stassinopoulos, A., and Goldberg, I. H. (1995) Specific binding of the biradical analogue of neocarzinostatin chromophore to bulged DNA: implications for thiol-independent cleavage, *Biochemistry 34*, 2267−2275.
16. Stassinopoulos, A., Ji, J., Gao, S., and Goldberg, I. H. (1996) Solution structure of a two-base DNA bulge complexed with an enediyne cleaving analogue, *Science 272*, 1943−1946.
17. Gao, X., Stassinopolous, A., Ji, J., Kwon, Y., Bare, S., and Goldberg, I. H. (2002) Induced formation of a DNA bulge structure by a molecular wedge ligand-post activated neocarzinostatin chromophore, *Biochemistry 41*, 5131−5143.
18. Wells, R. D. (1996) Molecular basis of genetic instability of triplet repeats, *J. Biol. Chem. 271*, 2875−2878.
19. Harvey, S. C. (1997) Slipped structures in DNA triplet repeat sequences: entropic contributions to genetic instabilities, *Biochemistry 36*, 3047−3049.
20. Loeb, L. A. (1998) Cancer cells exhibit a mutator phenotype, in *Advances in Cancer Research* (Vande Woude, G. F., and Klein, G., Eds.) Vol. 72, pp 25−56, Academic Press, New York.
21. Pearson, C. E., and Sinden, R. R. (1998) Slipped Strand DNA, Dynamic Mutations, and Human Disease, in *Genetic Instabilities and Hereditary Neurological Diseases* (Wells, R. D., and Warren, S. T., Eds.) pp 585−626, Academic Press, New York.
22. Kappen, L. S., Xi, Z., Jones, G. B., and Goldberg, I. H. (2003) Stimulation of DNA strand slippage synthesis by a bulge binding synthetic agent, *Biochemistry 42*, 2166−2173.
23. Vold, R. L., Waugh, J. S., Klein, M. P., and Phelps, D. E. (1967) Measurement of spin relaxation in complex systems, *J. Chem. Phys. 48*, 3831−3832.
24. Sklenar, V., Miyashiro, H., Zon, G., Miles, H. T., and Bax, A. (1986) Assignment of the ^{31}P and ^{1}H resonances in oligonucleotides by two-dimensional NMR spectroscopy, *FEBS Lett. 208*, 94−98.
25. Piotto, M., Saudek, V., and Sklenar, J. (1992) Gradient-tailored excitation for single-quantum NMR spectroscopy of aqueous solutions, *J. Biomol. NMR 2*, 661−665.
26. Delaglio, F., Grzesiek, S., Vuister, G. W., Zhu, G., Pfeifer, J., and Bax, A. (1995) NMRPipe: a multidimensional spectral processing system based on UNIX pipes, *J. Biomol. NMR 6*, 277−293.
27. Goddard, T. D., and Kneller, D. G. (2001) *SPARKY 3*, University of California, San Francisco.
28. Wuthrich, K. (1986) Resonance assignment strategy in nucleic acid (pp 224−246) and Resonance assignment strategy in protein (pp 117−161), *NMR of Proteins and Nucleic Acids*, John Wiley & Sons, New York.
29. Houser, R. V., Ravikumar, M., Chary, K. V. R., Sheth, A., Govil, G., Zu-Kun, T., and Miles, H. T. (1986) Solution structure of d-GAATTCGAATTC by 2D NMR. A new approach to determination of sugar geometries in DNA segments, *FEBS Lett. 205*, 71−76.
30. Kim, S.-G., Lin, L.-J., and Reid, B. R. (1992) Determination of nucleic acid backbone conformation by ^{1}H NMR, *Biochemistry 31*, 3564−3574.
31. Van Duynhoven, J. P. M., Goudriaan, J., Hilbers, C. W., and Wijmenga, S. S. (1992) Quantitative evaluation of TOCSY data. Application to sugar ring conformational analysis, *J. Am. Chem. Soc. 114*, 10055−10056.
32. Rinkel, L., and Altona, C. (1987) Conformational analysis of the deoxyribofuranose ring in DNA by means of sums of proton proton coupling constant: A graphical method, *J. Biomol. Struct. Dyn. 4*, 621−649.
33. Lankhorst, P. P., Haasnoot, C. A., Erkelens, C., and Altona, C. (1984) 1. Carbon-13 NMR in conformational analysis of nucleic

acid fragments. 2. A reparametrization of the Karplus equation for vicinal NMR coupling constants in CCOP and HCOP fragments, *J. Biomol. Struct. Dyn. 1*, 1387−1405.
34. Gorenstein, D. G., Schroeder, S. A., Fu, J. M., Metz, J. T., Roongta, V., and Jones, C. R. (1988) Assignments of ^{31}P NMR resonances in oligodeoxyribonucleotides: origin of sequence-specific variations in the deoxyribose phosphate backbone conformation and the ^{31}P chemical shifts of double-helical nucleic acids, *Biochemistry 27*, 7223−7237.
35. Brunger, A. T., Adams, P. D., Clore, G. M., DeLano, W. L., Gros, P., Grosse, K. R., Jiang, J. S., Kuszewski, J., Nilges, M., Pannu, N. S., Read, R. J., Rice, L. M., Simonson, T., and Warren, G. L. (1998) Crystallography & NMR System: A new software suite for macromolecular structure determination, *Acta Crystallogr. D54*, 905−921.
36. Keepers, J. W., and James, T. L. (1984) A theoretical study of distance determinations from NMR. Two-dimensional nuclear Overhauser effect spectra, *J. Magn. Reson. 57*, 404−426.
37. Lavery, R., and Sklenar, H. (1988) *J. Biomol. Struct. Dyn. 6*, 63−91.
38. Woodson, S. A., and Crothers, D. M. (1988) Preferential location of bulged guanosine internal to a G·C tract by proton NMR, *Biochemistry 27*, 436−445.
39. Morden, K. M., Gunn, B. M., and Maskos, K. (1990) NMR studies of a deoxyribodecanucleotide containing an extrahelical thymidine surrounded by an oligo(dA)·oligo(dT) tract, *Biochemistry 29*, 8835−8845.
40. Han, Z., and Gao, X. (2001) Sequence specific recognition of ligand-DNA complexes studied by NMR, *Curr. Med. Chem. 8*, 551−581.
41. Woodson, S. A., and Crothers, D. M. (1988) Binding of 9-aminoacridine to bulged-base DNA oligomers from a frame-shift hot spot, *Biochemistry 27*, 8904−8914.
42. Kalnik, M. W., Norman, D. G., Li, B. F., Swann, P. F., and Patel, D. J. (1990) Conformational transitions in thymidine bulge-containing deoxytridecanucleotide duplexes. Role of flanking sequence and temperature in modulating the equilibrium between looped out and stacked thymidine bulge states, *J. Biol. Chem. 265*, 636−647.
43. Woodson, S. A., and Crothers, D. M. (1988) Structural model for an oligonucleotide containing a bulged guanosine by NMR and energy minimization, *Biochemistry 27*, 3130−3141.
44. Joshua-Tor, L., Frolow, F., Appella, E., Hope, H., Rabinovich, D., and Sussman, J. L. (1992) Three-dimensional structures of bulge-containing DNA fragments, *J. Mol. Biol. 225*, 397−431.
45. Williams, L. D., and Goldberg, I. H. (1988) Selective strand scission by intercalating drugs at DNA bulges, *Biochemistry 27*, 3004−3011.
46. Gu, F., Xi, Z., and Goldberg, I. H. (2000) DNA damage by thiol-activated neocarzinostatin chromophore at bulged sites, *Biochemistry 39*, 4881−4891.
47. Kappen, L. S., Xi, Z., and Goldberg, I. H. (2001) Probing DNA single strands for single-base bulges with neocarzinostatin chromophore, *Biochemistry 40*, 15378−15383.
48. Kwon, Y., Xi, Z., Kappen, L. S., Goldberg, I. H., and Gao, S. (2003) New complex of post-activated neocarzinostatin chromophore with DNA: bulge DNA binding from the minor groove, *Biochemistry 42*, 1186−1198.

BI030072D